EPJ Web of Conferences **107**, 05001 (2016)
DOI: 10.1051/epjconf/201610705001

Impact of low-energy multipole excitations and pygmy resonances on radiative nucleon captures

N. Tsoneva[1,2,3,a], H. Lenske[2,4]

[1] *Frankfurt Institute for Advanced Studies (FIAS), D-60438 Frankfurt am Main, Germany*
[2] *Institut für Theoretische Physik, Universität Giessen, 35390 Giessen, Germany*
[3] *Institute for Nuclear Research and Nuclear Energy, 1784 Sofia, Bulgaria*
[4] *GSI Darmstadt, Darmstadt, Germany*

Abstract. Nuclear structure theory is considered in the framework of the development of a microscopic model for nucleon-capture astrophysical implementations. In particular, microscopically obtained strength functions from a theoretical method incorporating density functional theory and quasiparticle-phonon model are used as an input in a statistical reaction model. The approach is applied in systematic investigations of the impact of low-energy multipole excitations and pygmy resonances on dipole photoabsorption and radiative neutron- and proton-capture cross sections of key s- and r-process nuclei which is discussed in comparison with the experiment. For the cases of the short-lived isotopes ^{89}Zr and ^{91}Mo theoretical predictions are made.

1 Introduction

The nuclear electromagnetic (EM) response at excitation energies below and around the neutron threshold is a complex admixture of nuclear excitations of different origin. Among them of special importance are new modes of excitations called pygmy resonances which were theoretically predicted in medium and heavy nuclei with neutron excess and related to skin phenomena [1, 2]. These findings followed closely the observation of halos in light nuclei [3] and revealed new aspects of the isospin dynamics of nuclear matter.

Presently, the pygmy dipole resonance (PDR) has been detected experimentally in a variety of stable and unstable nuclei [4]. The rapidly increasing number of experiments, using different probes and techniques, allow for systematic studies of the PDR over isotopic and isotonic chains from different mass regions [5–13]. Furthermore, the implementation of complementary probes is found to be important for the understanding of the character of the low-energy EM strength which is highly fragmented.

Typically, in neutron-rich nuclei the PDR appears as an additional dipole strength component around the neutron threshold and situated on top of the low-energy tail of the giant dipole resonance (GDR) classically represented by a Lorentzian shape [14]. Theoretical analysis of transition densities and currents show that the observed PDR strength is very different from the giant dipole resonance (GDR) which dominates the electric dipole (E1) strength in atomic nuclei [4]. In this aspect standard strength functions (SF) based on Lorentz curves cannot describe the dipole strength distribution below the (γ, n) threshold correctly. However, microscopic nuclear structure models can provide a reliable description [15–23].

The most common explanation of the PDR is associated with oscillations of weakly bound single-particle neutron (for neutron-rich nuclei) or proton (for neutron-deficient nuclei) states from the nuclear surface layer with respect to isospin symmetric core.

The theoretical findings indicating the weak collectivity of this mode [16, 17, 21] are further confirmed by the measurements of total PDR strengths and corresponding contributions to energy-weighted-sum rules (EWSR) [5–7, 9–11, 13, 17]. Furthermore, from systematic studies of nuclear isotonic and isotopic chains, a correlation of total PDR strengths and nuclear skin thickness was found [5–7, 9–11, 13, 17]. In particular, the increase of the total PDR strength toward more neutron-rich nuclei can be addressed to the increase of the neutron skin thickness [5, 17, 24] which on the other hand is connected with the increase of the amount of those weakly bound neutron particle-hole (p-h) states around the Fermi surface. This can be further explained with the decrease of the neutron binding energy S_n and the increase of the absolute value of the difference between proton and neutron Fermi energies, $\Delta_F = \epsilon_p^F - \epsilon_n^F$. The latter is linearly correlated with the neutron skin thickness [4]. These results are extremely interesting as far as they give a link between the static properties of the nucleus related to the mean-field (MF) and the dynamics of low-energy nuclear excitations.

Recent theoretical studies reveal that the PDR has important impact on different processes of astrophysical aspects. In particular, it was found that the presence of PDR affects strongly neutron-capture reaction cross sec-

[a] e-mail: tsoneva@theo.physik.uni-giessen.de

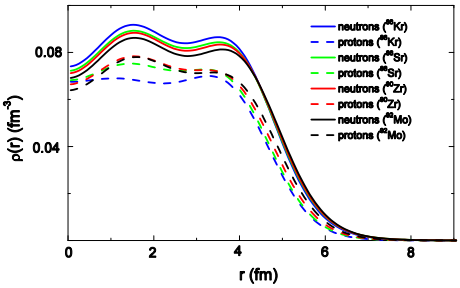

Figure 1. (Color online) Ground state densities in $N = 50$ isotones obtained by the phenomenological EDF + QPM approach.

tions of the stellar nucleosynthesis [25–28]. Furthermore, it was pointed out that the quasiparticle-random-phase-approximation (QRPA) which considers only coherent superpositions of two-quasiparticle (2QP) excitations, is not sufficient to account for the complexity of phenomena in the PDR region. Rather, an extended approach is required which explicitly accounts for the interactions among multi-quasiparticles and phonons. It can be successfully achieved in the framework of the quasiparticle-phonon model (QPM) [29].

Furthermore, the nuclear SF and especially its low-energy part is a very important ingredient for calculations of nuclear reaction rates [25]. Our recent investigations of the fine structure and dynamics of nuclear electric and magnetic dipole response functions show a very good description of experimental data [7, 9, 10, 13, 17, 25].

The presence of a neutron or proton skin affect as well excitations of other multipolarities and parities. In this connection, we investigated recently the quadrupole response of neutron-rich Sn nuclei up to 35 MeV [30]. Our approach, incorporating the energy-density functional (EDF) theory and the three-phonon QPM, was the first to predict the existence of pygmy quadrupole resonance (PQR) as a natural extension of the already known PDR for higher multipole excitations [30]. Meanwhile, these PQR states have been detected for the first time experimentally in ^{124}Sn nucleus via the (^{17}O,^{17}O'γ) reaction [31].

Here, we present new results on $E1$ SF in $N = 50$ isotones and ^{196}Pt which can be used to predict neutron-capture reaction cross sections within the formalism described in [25]. More specifically, the neutron-capture reactions ^{85}Kr(n,γ)^{86}Kr, ^{87}Sr(n,γ)^{88}Sr, ^{89}Zr(n,γ)^{90}Zr and ^{91}Mo(n,γ)^{92}Mo are studied with various predictions of the γ-SF and compared with available experimental data. For all these cases, the role of the PDR is examined and discussed in details. For the ^{89}Zr and ^{91}Mo nuclei which are hardly accessible experimentally, because of the short lifetime of the targets, radiative neutron-capture cross sections are theoretically predicted. Finally, the proton radiative capture reaction ^{89}Y(p,γ)^{90}Zr for which experimental data exist, is also studied to test the newly derived SF [25].

2 The theoretical approach

The theoretical approach is based on EDF theory [32] and QPM [29]. Our model Hamiltonian resembles in structure the standard QPM Hamiltonian [29] but in detail differs in the physical content in important aspects [16, 17]

$$H = H_{MF} + H_M^{ph} + H_{SM}^{ph} + H_M^{pp} \quad . \tag{1}$$

Here, $H_{MF} = H_{sp} + H_{pair}$ is treated by self-consistent Hartree-Fock-Bogoliubov (HFB) theory [32]. The term H_{sp} defines the independent motion of protons and neutrons in a static and spherically symmetric mean field and the term H_{pair} is a monopole pairing interaction in the particle-particle (pp) channel. The pure HFB picture is in fact extended beyond MF by dynamical self-energies, hence incorporating a more detailed spectral description of nuclear spectra. That goal is achieved in practice by taking advantage of the Kohn-Sham theorem of the EDF theory and applying fully microscopic HFB potentials and pairing fields as input [32]. Further a second step variation procedure is performed with scaled auxiliary potentials and pairing fields readjusted in a self-consistent manner such that nuclear ground state properties are well reproduced. In particular, obtained from this procedure nuclear binding energies, charge radii and the neutron skin thickness given by the differences of proton and neutron root-mean-square (rms) radii

$$\delta r = \sqrt{< r^2 >_n} - \sqrt{< r^2 >_p} \quad , \tag{2}$$

reproduce the results from Skyrme SLy4 HFB calculations [17] and the available experimental data of [33] within uncertainties below 1%. The total binding energy per nucleon, the mass, the charge radii and the related skin thicknesses as obtained by the EDF in N =50 isotones are compared with the data of [33] in Table 1.

H_M^{ph}, H_{SM}^{ph} and H_M^{pp} are residual interactions, taken as a sum of isoscalar and isovector separable multipole and spin-multipole interactions in the particle-hole (ph) and multipole pairing interaction in the pp channels. The model parameters are fixed either empirically [34] or by reference to QRPA calculation performed within the density matrix expansion (DME) of G-matrix interaction [32].

The reliable description of ground state properties is of genuine importance for extrapolations of QRPA and QPM calculations into unknown mass regions. In practice, for a given nucleus of mass A, Woods-Saxon potentials are adjusted in a self-consistent manner for protons and neutrons by the described above procedure (for details see also [32]). Furthermore, for the QPM calculations the monopole pairing is simplified by using a constant matrix element [16, 17]. The approach sketched above leads to a smooth dependence of the model parameters on A [17].

Calculations of ground state neutron and proton densities for N =50 are shown in Fig. 1. Of special importance are the nuclear surface regions which indicate clearly the formation of a neutron skin. A common observation is that the thickness of the neutron skin is related to the neutron-to-proton ratio N/Z in N =50 nuclei. Thus, the thickest

Table 1. HFB results obtained with the phenomenological EDF of the total binding energy, proton and neutron rms radii and the related to them skin thickness δr defined with Eq. (2) are compared to measured binding energies [33].

Nucleus	N/Z	$B(A)/A_{(EDF)}$, (MeV)	$B(A)/A_{(exp)}$, (MeV)	$\sqrt{< r^2 >_p}$, (fm)	$\sqrt{< r^2 >_n}$, (fm)	δr (fm)
^{86}Kr	1.39	-8.755	-8.712	4.131	4.264	0.133
^{88}Sr	1.32	-8.766	-8.733	4.185	4.291	0.106
^{90}Zr	1.25	-8.696	-8.710	4.229	4.303	0.074
^{92}Mo	1.19	-8.596	-8.658	4.269	4.325	0.056

neutron skin is found for the ^{86}Kr nucleus which has at the same time the largest N/Z ratio (see as well Table 1). Similar results were obtained in our studies of Z =50 and N =82 nuclei [5, 16, 17].

The nuclear excitations are expressed in terms of QRPA phonons [29]:

$$Q^+_{\lambda\mu i} = \frac{1}{2}\sum_{jj'}\left[\psi^{\lambda i}_{jj'}A^+_{\lambda\mu}(jj') - \varphi^{\lambda i}_{jj'}\widetilde{A}_{\lambda\mu}(jj')\right], \qquad (3)$$

where $j \equiv (nljm\tau)$ is a single-particle proton or neutron state; $A^+_{\lambda\mu}$ and $\widetilde{A}_{\lambda\mu}$ are time-forward and time-backward operators, coupling 2QP creation or annihilation operators to a total angular momentum λ with projection μ. The excitation energies of the phonons and the time-forward and time-backward amplitudes $\psi^{\lambda i}_{j_1j_2}$ and $\varphi^{\lambda i}_{j_1j_2}$ in Eq. (3) are determined by solving QRPA equations [29]. The formalism allows for a unified treatment of phonons with different collectivity.

Furthermore, we apply exact commutation relations between phonon creation and annihilation operators, thus preserving their internal fermionic structure. This is a necessary condition in order to satisfy the Pauli principle. Of great importance is that the QPM provides a microscopic approach to multiconfiguration mixing [29]. For the cases of spherical even-even nuclei considered here, the model Hamiltonian is diagonalized on an orthonormal set of wave functions constructed from one-, two- and three-phonon configurations which are implemented in the calculations of the EM transition matrix elements [35]. The latter incorporate transition operators accounting for the interaction of quasiparticles and phonons and their exact commutation relations [36].

3 Discussion

The appearance of PDR in the energy range below the neutron threshold is a general observation found in systematic EDF+QRPA and EDF+QPM calculations of the electric dipole response in different isotopic and isotonic chains of neutron-rich nuclei [5, 6, 9, 16, 17]. Here, we focus on the N = 50 isotones (see also Ref. [9]).

A common observation in nuclei with neutron skin [5, 6, 9, 16, 17] is that the total PDR strength obtained in EDF+QRPA calculations and the neutron skin thickness, δr are linearly correlated, as it is shown in Fig. 2 for N=50 isotones. This correlation is explained as follows. By definition the QRPA excited states are built only from single p-h contributions to the state vectors (see Eq. (3)). For neutron-rich nuclei, within the QRPA representation, the

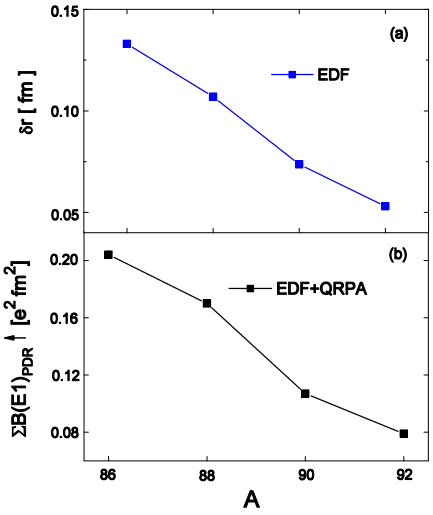

Figure 2. (Color online) N = 50 nuclei: (a) EDF calculations of neutron skin thickness δr as a function of A; (b) EDF+QRPA calculations of the total $B(E1)_{PDR}$ strength as a function of the mass number A. The summation is taken in the energy region below $E_\gamma \leq$9 MeV which is related to PDR [9, 17].

PDR is formed by a sequence of 1^- excited states, whose structure is dominated by oscillations of weakly bound, almost pure neutron 2QP configurations. Their contribution to transition matrix elements increases with the decrease of S_n.

Thus, from analyses of the structure of low-energy 1^- states and corresponding transition densities, the energy region below $E_\gamma \leq$9 MeV is related to the PDR and neutron skin oscillations [9, 17] whose total strength smoothly decreases with increasing proton number Z. With increasing excitation energies, the isovector dipole strength increases steadily, following closely the slope of the GDR which in data analyses is assumed to be of Lorentzian shape (see e.g. [14]). Theoretically, this can be seen in transition densities and state vectors structure which manifest an enlargement of the out-of-phase neutron to proton contributions and corresponding EWSR generally associated with the GDR [9, 17].

For comparison, we have performed two different kinds of QRPA calculations with respect to the nuclear MF and residual interactions used in the calculations of the nuclear excited states [25]. The first method includes nuclear MF determined by EDF formalism linked to self-

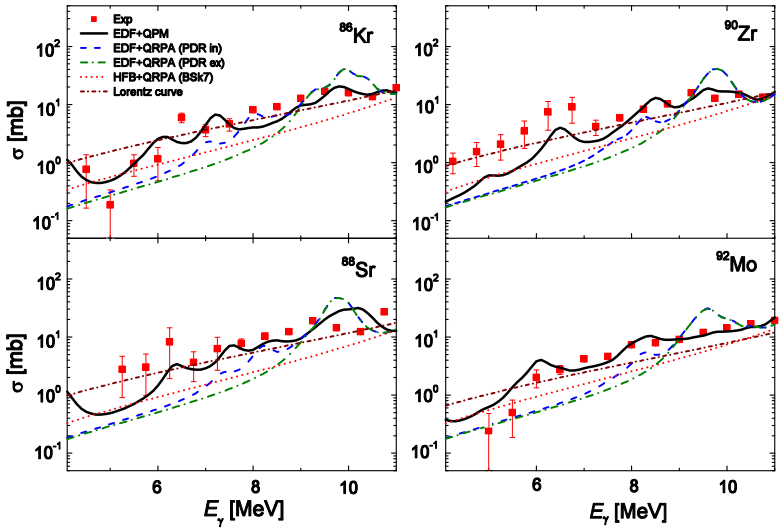

Figure 3. (Color online) Systematic EDF+QRPA including PDR (blue dashed line), EDF+QRPA excluding PDR (green long-dash-dot line), three-phonon EDF+QPM (black solid line), HFB+QRPA calculation based on the BSk7 force (red dotted line) and standard Lorentz curves (brown short-dash-dot line) with parameter sets from Table 1 calculations of dipole photoabsorption cross section below the neutron threshold of $N = 50$ nuclei in comparison with experimental data [9].

consistent Skyrme (SLy4) HFB calculations and the separable residual interactions of the QPM which are explained in [17, 29]. The second approach, is based on a self-consistent HFB+QRPA model [37] which incorporates BSk7 Skyrme force [**?**]. In this case, the MF and the residual interaction are derived consistently from the Skyrme (BSk7) EDF as discussed in in Refs. [25, 37]. The two methods are found to give similar results for the dipole photoabsorption cross sections in $N = 50$ nuclei (see in Fig. 3). In addition, a comparison of EDF+QRPA calculations of dipole photoabsorption cross sections obtained in two different cases, when the PDR is included (PDR in) or excluded (PDR ex) is shown in Fig. 3. The EDF+QRPA (PDR in) findings point out that the PDR has a peak in the dipole photoabsorption cross section at about $E_\gamma = 8$ MeV which smoothly moves up to higher excitation energy towards ^{92}Mo. More specifically, the EDF+QRPA (PDR in) calculation in ^{86}Kr gives a 56% increase of the total dipole photoabsorption cross section in the PDR energy region compared to the EDF+QRPA (PDR ex) calculations. The effect gradually reduces with the increase of the proton number Z reaching about 25% in ^{92}Mo. A comparison between the theoretical results and experimental data is also shown in Fig. 3. It is seen that in general all QRPA results underestimate significantly the low-energy dipole photoabsorption data. Furthermore, QRPA calculations as well as standard Lorentzian approximations (also given in Fig. 3) are not able to describe in detail the complex dynamics of the low-energy dipole response function due to the interference of low-energy multi-phonon, PDR and GDR states (see in Ref. [25] for more details). The description of the experimental data can be significantly improved if the interaction between quasiparticles and phonons [29] is taken into account in the framework of the three-phonon EDF+QPM which is shown in Fig. 3. It indicates that in the PDR region the coupling of QRPA PDR and GDR phonons and multi-phonon states is very important. The result is a shift of the $E1$ strength to lower energies which can be described in the three-phonon QPM formalism also quantitatively [9].

Our EDF+ QRPA and three-phonon QPM microscopic SF-s have been implemented into the TALYS reaction code to investigate the ^{85}Kr(n,γ)^{86}Kr cross sections of astrophysical relevance [26]. It was found that the neutron-capture cross section calculated within the EDF+three-phonon QPM is in very good agreement with experimental data [26] while the one calculated within the EDF+QRPA formalism underestimates the data by about 35%.

Here, we extend our studies by analyzing systematically the neutron-capture reactions in $N = 50$ isotones for the additional ^{87}Sr(n,γ)^{88}Sr, ^{89}Zr(n,γ)^{90}Zr and ^{91}Mo(n,γ)^{92}Mo reactions. TALYS calculations are performed using the $E1$ SF-s from EDF+QRPA (SLy4) with PDR contributions (PDR in) and without PDR contributions (PDR ex) in order to investigate the PDR impact on the cross section. The contribution of the PDR to radiative capture cross section for 10–100 keV incident neutrons is estimated to be of the order of $\sim$ 50% for ^{85}Kr(n,γ)^{86}Kr, $\sim$ 22% for ^{87}Sr(n,γ)^{88}Sr, $\sim$ 13% for ^{89}Zr(n,γ)^{90}Zr and $\sim$ 10% for ^{91}Mo(n,γ)^{92}Mo, as shown in Fig. 4.

As far as the QPM predictions are concerned, it can be seen in Fig. 4 that it leads to radiative neutron-capture

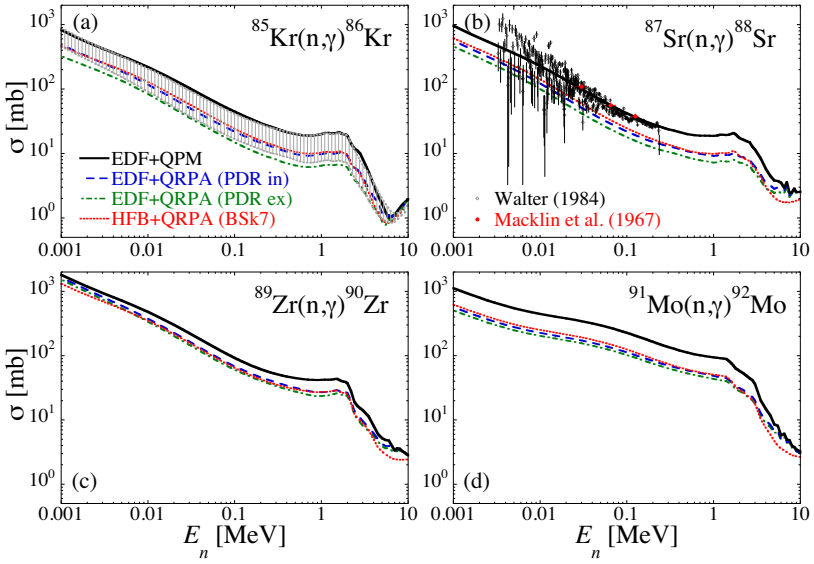

Figure 4. (Color online) Ground-state neutron-capture cross sections of (a) ^{85}Kr(n,γ)^{86}Kr, (b) ^{87}Sr(n,γ)^{88}Sr, (c) ^{89}Zr(n,γ)^{90}Zr and (d) ^{91}Mo(n,γ)^{92}Mo calculated with TALYS using EDF plus three-phonon QPM (black solid line), EDF+QRPA (PDR included) (blue dashed line), EDF+QRPA (PDR excluded) (green dash-dot line), and HFB+QRPA (BSk7) (red dotted line) strength functions. For ^{85}Kr(n,γ)^{86}Kr, the hashed area corresponds to the cross section determined with the experimental strength as derived in Ref. [26]. For ^{87}Sr(n,γ)^{88}Sr, TALYS cross sections are compared with experimental data [25].

cross sections higher than the one obtained on the basis of the QRPA strength by a factor of about 2 (or slightly less in the ^{89}Zr(n,γ)^{90}Zr case). The higher cross section with the QPM strength is directly related to the enhanced strength stemming from the phonon coupling below the neutron threshold (Fig. 3). It should be recalled that in radiative neutron-capture cross section for incident neutrons with keV energies, the γ energies of relevance are found below the neutron separation energies [25]. In the case of the QPM, the major contribution to the ^{85}Kr and ^{87}Sr neutron-capture cross section originates from the SF around 4 MeV photons. This energy range has a dominant core polarization counterpart [25].

Recently, ^{195}Pt(p, p'γ)^{195}Pt and ^{195}Pt(d, pγ)^{196}Pt reactions were carried out at the Oslo Cyclotron Laboratory using deuteron and proton beams accelerated to 11.3 MeV and 16.5 MeV, respectively. Furthermore, for the first time, it was possible to determine the detailed shape of these resonances for excitation energies in the quasicontinuum. For the explanation of the experiment theoretical calculations in the frame of our EDF+QPM approach are done. The preliminary results obtained from the calculations of dipole SF in ^{196}Pt are found in very good agreement with the Oslo data [38]. These new investigations will contribute to the study of the r-process of nucleosynthesis.

An important question to clarify is the fine structure of the observed low-energy dipole strengths. For this purpose, three-phonon QPM calculations of low-energy $E1$ and spin-flip $M1$ excitations in ^{52}Cr, ^{90}Zr and ^{138}Ba nuclei are made. The results are compared to experimental data obtained from polarized photon beams [7, 10, 13]. Both, experiment and theory show the predominantly electric character of the observed low-energy dipole strength.

To test the newly derived SF-s in N=50 nuclei, it is also of particular interest to study the radiative proton-capture reaction ^{89}Y(p,γ)^{90}Zr recently re-measured in Ref. [39, 40]. In this case, the cross section becomes sensitive to the γ-SF essentially above the neutron emission threshold around 3.6 MeV. Below this threshold, the cross section is only sensitive to the proton-nucleus optical potential [25]. As shown in Fig. 5, the QPM model allows for a significantly better description of the cross section above 4 MeV, at least for the adopted HFB plus combinatorial nuclear level density (NLD) model [25]. The QRPA models lead to a substantial underestimation of the cross section and the PDR contribution is found to have a rather small impact of no more than 5 to 10%. In conclusion, the present work reveals the predictive power of an advanced microscopic nuclear structure model based on the self-consistent EDF theory and QPM in systematic studies of dipole photoabsorption and radiative nucleon-capture cross sections of key s- and r- process nuclei. In particular, the contribution of the PDR to dipole photoabsorption and neutron-capture cross sections at astrophysical energies is theoretically investigated in N = 50 and ^{196}Pt nuclei. The results obtained with the EDF+QRPA approach in N = 50 isotones indicate that the largest PDR impact, of the order of $\sim$ 50%, is observed for the ^{85}Kr(n,γ)^{86}Kr reaction where the target nucleus ^{85}Kr has the largest N/Z=1.43 ratio. The effect smoothly decreases with the decrease of the N/Z ratio towards ^{91}Mo (N/Z=1.22) and its contribution to the ^{91}Mo(n,γ)^{92}Mo reaction cross section is of about 10% [25]. This is similar to the PDR contribution to the

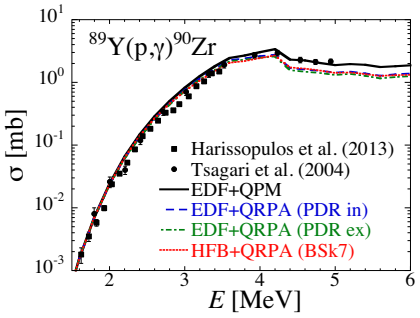

Figure 5. (Color online) Radiative proton-capture cross section ^{89}Y(p,γ)^{90}Zr calculated with TALYS using EDF plus three-phonon QPM (black solid line), EDF+QRPA (PDR included) (blue dashed line), EDF+QRPA (PDR excluded) (green dash-dot line), and HFB+QRPA(BSk7) (red dotted line) SF-s [25].

corresponding dipole photoabsorption cross sections. The PDR impact to the radiative proton-capture cross section for the ^{89}Y(p,γ)^{90}Zr reaction is found to be small, less than $\sim 10\%$.

These studies clearly indicate that the QRPA is not sufficient to account for the nuclear excitations below the neutron threshold and hence QRPA SF-s will in general underestimate by a factor of about 2 radiative capture cross sections at astrophysical energies (see also [25]). However, three-phonon QPM calculations provide a good description of experimental data, thus indicating the ability of the microscopic multi-phonon theory for exploratory investigations of nuclear reaction rates in hitherto experimentally inaccessible mass regions.

Acknowledgements

This work was financially supported by BMBF, contract 05P12RGFTE, and Helmholtz International Center for FAIR within the framework of the LOEWE program (application Nr. 2696).

References

[1] Y. Suzuki *et al.*, Prog. Theor. Phys. **83**, 180 (1990)
[2] P. Van Isacker *et al.*, Phys. Rev. C **45**, R13 (1992)
[3] I. Tanihata *et al.*, Phys. Rev. Lett. **55**, 2676 (1985)
[4] D. Savran *et al.*, Prog. Part. and Nucl. Phys. **70**, 210 (2013) and refs. therein.
[5] S. Volz *et al.*, Nucl. Phys. A **779**, 1 (2006)
[6] R. Schwengner *et al.*, Phys. Rev. C **78** 064314 (2008)
[7] A. P. Tonchev *et al.*, Phys. Rev. Lett. **104**, 072501 (2010)
[8] H.K. Toft *et al.*, Phys. Rev. C **83**, 044320 (2011)
[9] R. Schwengner *et al.*, Phys. Rev. C **87**, 024306 (2013)
[10] G. Rusev *et al.*, Phys. Rev. Lett. **110**, 022503 (2013)
[11] F.C.L. Crespi *et al.*, Phys. Rev. Lett. **113**, 012501 (2014)
[12] B. Özel-Tashenov *et al.*, Phys. Rev. C **90**, 024304 (2014)
[13] Krishichayan *et al.*, Phys. Rev. C **91**, 044328 (2015)
[14] B. L. Berman, At. Data Nucl. Data Tables **15**, 319 (1975)
[15] D. Vretenar *et al.*, Nucl. Phys. A **692** 496 (2001)
[16] N. Tsoneva *et al.*, Phys. Lett. B **586** 213 (2004)
[17] N. Tsoneva *et al.*, Phys. Rev. C **77** 02431 (2008) and refs. therein.
[18] T. Hartmann *et al.*, Phys. Rev. Lett. **93**, 192501 (2004)
[19] D. Sarchi *et al.*, Phys. Lett. B **601** 27 (2004)
[20] J. Piekarewicz, Phys. Rev. C **73**, 044325 (2006)
[21] P.-G. Reinhard *et al.*, Phys. Rev. C **87**, 014324 (2013)
[22] E. Litvinova *et al.*, Phys. Rev. C **88**, 044320 (2013)
[23] F. Knapp *et al.*, Phys. Rev. C **90**, 014310 (2014)
[24] J. Piekarewicz, Phys. Rev. C **83**, 034319 (2011)
[25] N. Tsoneva *et al.*, Phys. Rev. C **91**, 044318 (2015) and refs. therein.
[26] R. Raut *et al.*, Phys. Rev. Lett. **111**, 112501 (2013)
[27] A. Avdeenkov *et al.*, Phys. Rev. C **83**, 064316 (2011)
[28] E. Litvinova *et al.*, Nucl. Phys. A **823** 26 (2009)
[29] V.G. Soloviev, *Theory of complex nuclei* (Oxford: Pergamon Press, 1976)
[30] N. Tsoneva *et al.*, *Phys. Lett. B* **695**, 174 (2011)
[31] L. Pellegri *et al.*, Phys. Rev. C **92**, 014330 (2015)
[32] F. Hofmann *et al.*, Phys. Rev. C **57**, 2281 (1998)
[33] G. Audi *et al.*, Chin. Phys. C **36**, 1287 (2012)
[34] A. Vdovin *et al.*, Phys. Elem. Part. At. Nucl., 14, 237 (1983)
[35] M. Grinberg *et al.*, Nucl. Phys. A **573**, 231 (1994)
[36] V.Yu. Ponomarev *et al.*, Nucl. Phys. A **635**, 470 (1998)
[37] S. Goriely *et al.*, Nucl. Phys. A **706**, 217 (2002)
[38] F. Giacoppo *et al.*, to be submitted.
[39] S. Harissopulos *et al.*, Phys. Rev. C **87**, 025806 (2013)
[40] L. Netterdon *et al.*, Phys. Lett. B **744**, 358 (2015)